VOLUME VELOCITY VIBRATION CONTROL OF A SMART PANEL USING A QUADRATICALLY SHAPED PVDF ACTUATOR AND MULTIPLE ACCELEROMETERS

Y-S Lee University of Southampton, ISVR, Southampton
P Gardonio University of Southampton, ISVR, Southampton
S J Elliott University of Southampton, ISVR, Southampton

1. INTRODUCTION

High frequency sound transmission control through panels can be achieved with passive control methods such as mass-damping and stiffness treatments [1,2]. At low frequencies, active control methods have been applied effectively [3,4,5,6]. This paper presents a theoretical and experimental study of low frequency feedback control of sound transmission through a panel based on active structural acoustical control (ASAC) [4,7]. ASAC systems [4] utilise structural actuators that are driven to minimise the overall sound radiation/transmission of the panel that could be either estimated with a set of acoustic sensors placed in the radiating area or indirectly with structural sensors.

Johnson and Elliott [8] have shown that the net volume velocity of a panel is a good estimator of the low frequency sound radiation. Indeed at low frequency the volumetric vibration of the panel corresponds to the first radiation mode. Radiation modes radiate sound independently and therefore by cancelling the volumetric vibration of the panel the low frequency sound radiation can be controlled. Volume velocity has been measured in practice using structural sensors, as for example arrays of quadratically shaped PVDF strips [8,9], variable width PVDF strips [10] and arrays of piezoelectric patches [11]. These structural sensors provide a single output proportional to the volume velocity vibration of a panel that could be used to implement single channel direct velocity feedback control (DVFB) using a matched and collocated uniform force piezoelectric actuator [12,13].

A feedback control system with a collocated actuator-sensor could give considerable advantages for DVFB, such as robust stability and very high performance with the DVFB control scheme. If a collocated sensor/actuator pair is used, the plant transfer function would be proportional to the input mobility of the structure, which must have a positive real part. Also if the feedback controller has a positive real part, then the open-loop transfer function must stay in the right-hand half of the Nyquist diagram and so the system is unconditionally stable [14].

A *matched* piezoelectric sensor/actuator pair with a quadratically shaped PVDF actuator for uniform transverse force excitation on a panel is expected to offer strictly positive real (SPR) property [8,13]. However it has been found that the transfer function of a matched piezoelectric actuator/sensor pair suffers from non-SPR property due to *in-plane motion coupling* with the transverse motion [13,15].

Several solutions to this problem have been suggested. For examples, Cole et al [16] have proposed a system with two matched transducers (*sensoriactuators*) that work simultaneously as sensors and actuators or Yang and Huang [17] have proposed a four-layer arrangement of piezoelectric transducers. Unfortunately, the method using a pair of matched sensoriactuators requires complex circuits to compensate for the capacitance of the piezoelectric element and is therefore difficult to implement in practice [18,19]. The four-layer configuration has shown inter-layer coupling between piezoelectric transducers bonded adjacently and causes severe coupled detection mechanism [20].

Maillard and Fuller [21] have suggested to measure volume velocity vibration with an array of accelerometers so that the in-plane coupling phenomenon for the detection of volume velocity is avoided. The net volume velocity can be measured by summing up the signal from an array of accelerometers evenly distributed on a panel.

For this study, a smart panel with a uniform force strain actuator made with a quadratically shaped PVDF film on one side and an array of accelerometer-sensors on the other side has been constructed. This smart panel has been mounted on the top side of a wooden box, which has a loudspeaker inside which acts as a primary disturbance source. The theoretical description on the quadratically shaped PVDF actuator and the volume velocity sensor used in this study is given in section 2 and 3. Section 4 describes the configuration of the experimental smart panel system with a SISO feedback controller and section 5 shows the analytical modelling

of the plant response. Section 6 discusses the measured and calculated plant frequency response functions (FRF) when the PVDF actuator shaping error effects are modelled. Then results on the vibration and acoustic feedback control are discussed in Section 7.

2. OUT-OF-PLANE UNIFORM FORCE ACTUATOR

The *out-of-plane uniform force actuator* considered in this section can be regarded as a composite structure consisting of piezoelectric film with very thin electrodes on both sides. When a voltage is applied between the two electrodes, an electric field is generated across the piezoelectric material which therefore deforms by means of the inverse piezoelectric effect. When such a piezoelectric actuator is bonded to the surface of a panel the inverse piezoelectric effect produces a distributed force field on the surface of the panel so that the panel will be bent, twisted and stretched.

The strain/stress relationships for the piezoelectric actuator with a spatial sensitivity function $S(x,y)$ can be derived from the piezoelectric material constitutive equation which is given by the following relation [22]:

$$\begin{Bmatrix} \sigma_x^{pe} \\ \sigma_y^{pe} \\ \sigma_{xy}^{pe} \end{Bmatrix} = \mathbf{C} \begin{Bmatrix} \varepsilon_x \\ \varepsilon_y \\ \varepsilon_{xy} \end{Bmatrix} - S(x,y) \begin{Bmatrix} e_{31} \\ e_{32} \\ e_{36} \end{Bmatrix} \frac{V_3(t)}{h_{pe}}, \tag{1}$$

where $\sigma_x^{pe}, \sigma_y^{pe}, \sigma_{xy}^{pe}$ and $\varepsilon_x, \varepsilon_y, \varepsilon_{xy}$ are the stress and strain components in the $x-$ and $y-$directions and $x-y$ plane of the piezoelectric material and the matrix $\mathbf{C}$ is defined with

$$\mathbf{C} = \begin{bmatrix} Y_{pe}/(1-\nu_{pe}^2) & \nu_{pe}Y_{pe}/(1-\nu_{pe}^2) & 0 \\ \nu_{pe}Y_{pe}/(1-\nu_{pe}^2) & Y_{pe}/(1-\nu_{pe}^2) & 0 \\ 0 & 0 & Y_{pe}/2(1+\nu_{pe}) \end{bmatrix}. \tag{2}$$

Y_{pe} and ν_{pe} represent the Young's modulus and the Poisson's ratio of the piezoelectric material. The piezoelectric stress constant terms e_{ij} and the piezoelectric strain constant terms d_{ij} are linked by the relation: $[e_{31} \quad e_{32} \quad e_{36}]^T = \mathbf{C}[d_{31} \quad d_{32} \quad d_{36}]^T$, where the indices 1, 2, 3 are the principal axes of the piezoelectric material and the index 6 is the plane 1-2, when the voltage is applied across the direction 3 [23]. The lossless out-of-plane motion of a homogenous and isotropic panel can be expressed [24] as

$$\frac{\partial^2 M_x}{\partial x^2} + 2\frac{\partial^2 M_{xy}}{\partial x \partial y} + \frac{\partial^2 M_y}{\partial y^2} = m\frac{\partial^2 w}{\partial t^2} - p(x,y,t) \tag{3}$$

where $m = 2\rho_s h_s$ is the mass per unit area of the panel, ρ_s is the density of the panel material and $p(x,y,t)$ is the distributed out-of-plane loading. When the piezoelectric actuator is bonded on the surface of the panel under a given stress field, then the moments M_x, M_y, and M_{xy} are given by the following relations:

$$\begin{aligned} M_x &= \int_{-h_s}^{h_s} \sigma_x^s z dz + \int_{h_s}^{h_s+h_{pe}} \sigma_x^{pe} z dz \\ M_y &= \int_{-h_s}^{h_s} \sigma_y^s z dz + \int_{h_s}^{h_s+h_{pe}} \sigma_y^{pe} z dz \\ M_{xy} &= \int_{-h_s}^{h_s} \sigma_{xy}^s z dz + \int_{h_s}^{h_s+h_{pe}} \sigma_{xy}^{pe} z dz, \end{aligned} \tag{4}$$

where h_s is the half-thickness of the panel and h_{pe} is the thickness of the piezoelectric actuator. Assuming both the panel and the piezoelectric actuator to be thin plates, then the stress-strain relationships, in the absence of an electric field for the piezoelectric actuator, are given by [24]

(5)

$$\sigma_x^s = \frac{Y_s}{1-\nu_s^2}(\varepsilon_x + \nu_s \varepsilon_y) \qquad \sigma_y^s = \frac{Y_s}{1-\nu_s^2}(\varepsilon_y + \nu_s \varepsilon_x) \qquad \sigma_{xy}^s = \frac{Y_s}{2(1-\nu_s^2)}\varepsilon_{xy}$$

where $\sigma_x^s, \sigma_y^s, \sigma_{xy}^s$ and $\varepsilon_x, \varepsilon_y, \varepsilon_{xy}$ are the stress and strain components in the *x*- and *y*-directions and *x*-*y* plane; Y_s and ν_s represent the Young's modulus and the Poisson's ratio of the panel. If the smart rectangular panel is excited only in flexure, then the strains throughout the plate and piezoelectric actuator will be equal to

$$\varepsilon_x = -z\frac{\partial^2 w}{\partial x^2} \qquad \varepsilon_y = -z\frac{\partial^2 w}{\partial y^2} \qquad \varepsilon_{xy} = -2z\frac{\partial^2 w}{\partial x \partial y} \tag{6}$$

where $\varepsilon_x, \varepsilon_y, \varepsilon_{xy}$ are either the plate or piezoelectric material strain components in the $x-$ and $y-$directions and $x-y$ plane. When the piezoelectric actuator is excited by an input voltage $V_3(t)$, the forced equation for the out-of-plane motion of the panel can be derived from equations (1), (3), (4), (5) and (6) to be

$$(D_s + D_{pe})\left(\frac{\partial^4 w}{\partial x^4} + 2\frac{\partial^4 w}{\partial x^2 \partial y^2} + \frac{\partial^4 w}{\partial y^4}\right) + m\frac{\partial^2 w(t)}{\partial t^2} = -h_{act} V_3(t) L_{pe}[S(x,y)] + p(x,y,t) \tag{7}$$

where $h_{act} = h_s + h_{pe}/2$. The Laplacian operator describing the transverse excitation on the panel is given by

$$L_{pe}[S(x,y)] = e_{31}\frac{\partial^2 S(x,y)}{\partial x^2} + 2e_{36}\frac{\partial^2 S(x,y)}{\partial x \partial y} + e_{32}\frac{\partial^2 S(x,y)}{\partial y^2} \tag{8}$$

and D_s and D_{pe} are given by the following expressions

$$D_s = \frac{2Y_s h_s^3}{3(1-\nu_s^2)} \qquad D_{pe} = \frac{Y_{pe}(h_{pe}^3 + 3h_{pe}h_s^2 + 3h_{pe}^2 h_s)}{3(1-\nu_{pe}^2)} \tag{9}$$

The condition necessary to generate an out-of-plane uniform force is to have a piezoelectric material with constant sensitivity function along the *y*-direction and quadratic sensitivity along the *x*-direction [25]:

$$S(x,y) = -k(x^2 - L_x x) \tag{10}$$

where *k* is a constant so that $S(0,y) = 0$ and $S(L_x,y) = 0$. By differentiating the sensitivity function in the *x*-direction twice, it can be found that:

$$\frac{\partial^2 S(x,y)}{\partial x^2} = \text{constant} = -2k \qquad \frac{\partial^2 S(x,y)}{\partial y^2} = 0 \tag{11}$$

Substituting these values into equation (8) and assuming the piezoelectric stress constant e_{36} to be negligible [22], then the resulting distributed out-of-plane uniform force $f_u(t)$, per unit surface area is found to be [13]

$$f_u(t) = -h_{act} V_3(t) L_{pe}[S(x,y)] = 2h_{act} e_{31} k V_3(t). \tag{12}$$

When e_{31}=0.052 [$NV^{-1}m^{-1}$], *k*=16.903 and h_{act}=0.00075 [m], a uniform force of about 0.13 Pa can be induced over the smart panel with 100V.

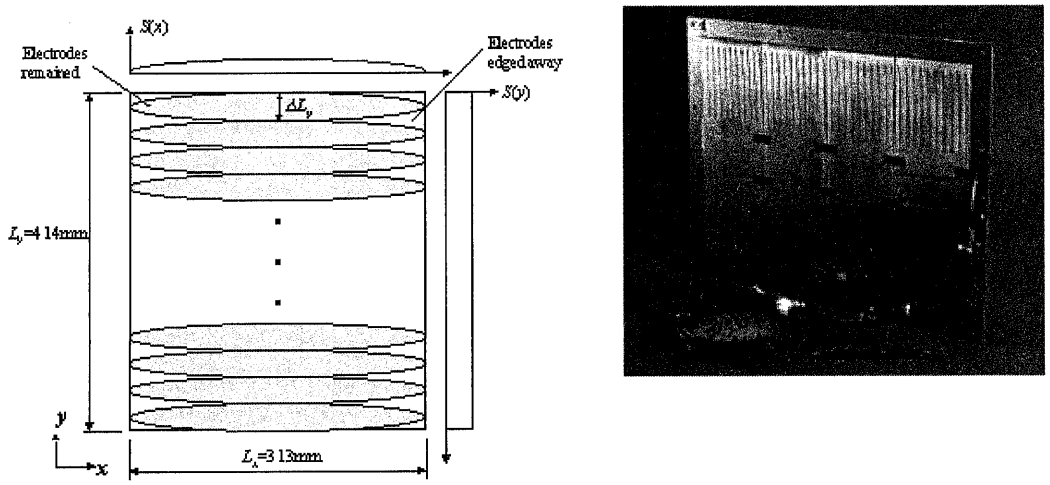

(a) (b)

Figure 1 (a) Arrangement of a distributedly collocated quadratically shaped piezoelectric PVDF actuator and sensor pair bonded on both sides of a rectangular plate. (b) A smart panel manufactured.

The shaping shown in Figure 1 gives, in first approximation, a set of line forces along the axis centreline of each strip [13]. This type of excitation approximates quite well a uniform force if the width ΔL_y of each strip is sufficiently small compared with the wavelength of the panel out-of-plane bending modes. The geometry and physical properties of the panel and the PVDF film for the uniform force actuator is given in Table 1.

3. ACCELEROMETERS ARRAY VOLUME VELOCITY SENSOR

The radiated sound power from the panel can be estimated by considering the vibration of the panel as made of a finite number of elemental acoustic radiators, each of which acts as a monopole source. The total radiated sound power can then be expressed in terms of the out-of-plane complex velocity vector $\mathbf{v}$ of the radiating elements as [8]

$$W = \mathbf{v}^H \mathbf{R} \mathbf{v}, \tag{13}$$

Table 1. Geometry and physical properties of the panel and PVDF film.

	plate	PVDF film
Dimension (length × width)	$L_x \times L_y = 313 \times 414$ mm (aluminium)	$L_x \times \Delta L_y = 313 \times 10$ mm (Forty quadratically shaped strips)
Thickness	$2h_s = 1$ mm	$h_{pe} = 0.5$ mm
Mass density	$\rho_s = 2700$ kgm^{-3}	$\rho_s = 1780$ kgm^{-3}
Young's modulus	$Y_s = 7.1 \times 10^{10}$ Nm^{-2}	$Y_{pe} = 2.0 \times 10^9$ Nm^{-2}
Poisson ratio	$\nu_s = 0.33$	$\nu_{pe} = 0.31$
Histeresis loss factor	$\eta_s = 0.05$	$\eta_{pe} = 0.05$

where $\mathbf{R}$ is the radiation resistance matrix and the superscript *H* denotes the Hermittian transpose. The matrix $\mathbf{R}$ is positive definite because the power output must be greater than zero unless the velocity is zero. The diagonal and off-diagonal terms of the matrix $\mathbf{R}$ represent the *self-radiation resistances* and the *mutual-radiation resistances* respectively. Since the out-of-plane velocity of the surface can be expressed as $v(x,y) = \sum_{n=1}^{N} a_n \phi_n(x,y)$, where a_n and ϕ_n are the amplitude and excitation factor for the *n-th* mode respectively. Thus the sound power *W* radiated by the panel then can be expressed by multiplying an *N*-length complex amplitude vector $\mathbf{a}$ by a finite $N \times N$ matrix $\mathbf{M}$ of self- and mutual-radiation resistances of the structural modes, as

$$W = \mathbf{a}^H \mathbf{M} \mathbf{a} . \tag{14}$$

Since the matrix $\mathbf{M}$ is normal, the following eigenvector/eigenvalue decomposition

$$\mathbf{M} = \mathbf{\Phi}^H \mathbf{\Omega} \mathbf{\Phi} \tag{15}$$

can be implemented where $\mathbf{\Phi}$ is an $N \times N$ unitary matrix of orthogonal real eigenvectors, and $\mathbf{\Omega}$ is a diagonal matrix with the correspective eigenvalues. Using equations (13), (14) and (15), the total radiated sound power can now be expressed [8],

$$W = \mathbf{b}^H \mathbf{\Omega} \mathbf{b} = \sum_{n=1}^{N} \Omega_n |b_n|^2 , \tag{16}$$

where a vector of transformed radiation mode amplitude $\mathbf{b}$ is given as [26]

$$\mathbf{b} = \mathbf{\Phi} \mathbf{a} , \tag{17}$$

and b_n represents the amplitude of the *n-th* radiation mode. Radiation modes radiate sound *independently* [26]. At low frequencies the sound radiation is controlled by the first radiation mode which approximately corresponds to the volumetric vibration of the panel. The volume velocity of a harmonically vibrating plate ($L_x \times L_y \times 2h_s$) is expressed analytically as

$$Q(\omega) = j\omega \left[\int_0^{L_x} \int_0^{L_y} w(x, y, \omega) dx dy \right], \tag{18}$$

where $w(x, y, \omega)$ is the flexural displacement of the plate.

The smart panel shown in Figure 1 has been designed with a matched quadratically shaped PVDF actuator/sensor pair to make a plant transfer function to be *strictly positive real* (SPR) [27]. However, the matched pair did not provide SPR property due to the in-plane motion coupling as shown in Figure 2 [13,15]. As described in references [13,15], the measured FRF with the matched pair as shown in Figure 2, suffers from an increasing trend of magnitude with the increase of frequency, and a phase lag at about 12000Hz that exceeds -90° so that the sensor-actuator FRF is not SPR. In order to avoid this coupling problem between the sensor and the actuator an array of 16 accelerometers evenly distributed over the panel surface has been used to detect the volume velocity vibration of the panel. The 16 accelerometers are arranged a 4×4 array every 1/8, 3/8, 5/8, 7/8 of L_x and L_y of the smart panel.

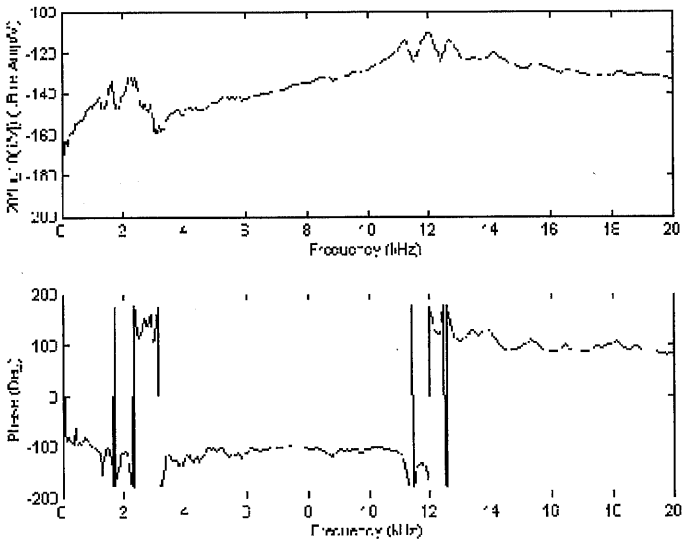

Figure 2. Measured FRF (0 - 20000Hz) of a smart panel with a matched quadratically shaped PVDF actuator/sensor pair which suffers from in-plane motion coupling.

4. SMART PANEL WITH A SISO FEEDBACK CONTROLLER

The panel with the 4×4 array of accelerometers and the piezoelectric actuator is clamped on a wooden box as can be seen from Figure 3(a). A loudspeaker is installed inside the box to generate primary disturbance noise on the panel.

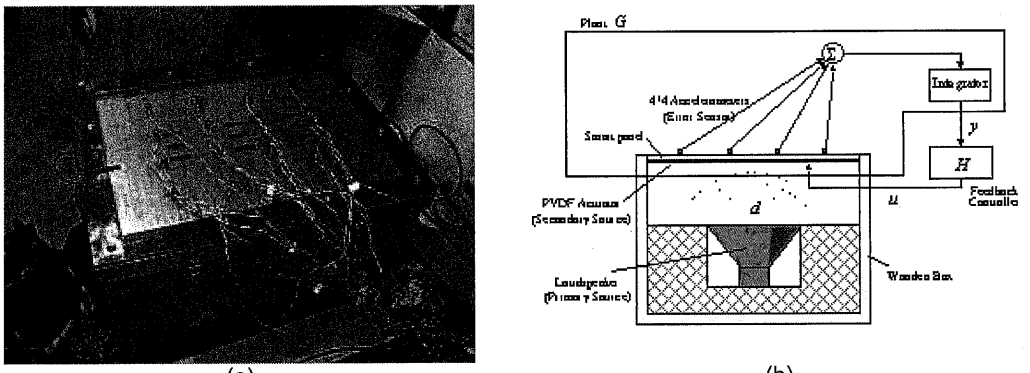

(a) (b)

Figure 3. (a) Experimental set-up of a smart panel consisting of an array of PVDF actuators and a 4*4 accelerometers array. (b) Velocity feedback control scheme.

The 16 PCB accelerometers (Model A352C67) are connected to a PCB 16-channel signal conditioner (Series 481A) that sums all the 16 signals together. This signal is then integrated through a PCB integrator (Model 480B10) to generate a velocity signal. The resulting single input single output sensor/actuator system has been connected to a SISO feedback control system as shown in Figure 3(b).

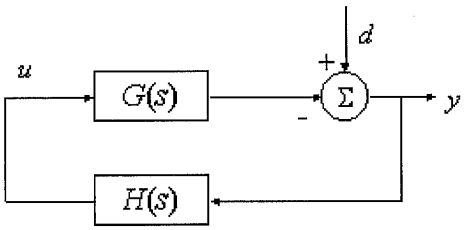

Figure 4. A single-channel feedback control system for disturbance rejection.

As shown in Figure 3(b) and summarised in the block diagram in Figure 4, the testing system considered is composed by a smart panel characterised by its plant response $G(s)$, a controller $H(s)$ and a primary source (loudspeaker). The plant $G(s)$ includes the panel, a secondary source (PVDF actuator) and an error sensor (accelerometer array). If the feedback control system is stable, the spectrum of the error sensor output $y(j\omega)$ is related to that of the sensor output before control, $d(j\omega)$, by the expression [14]

$$y(j\omega) = [1+G(j\omega)H(j\omega)]^{-1}d(j\omega). \tag{19}$$

For this control scheme, the control input to the secondary source (actuator), $u(j\omega)$, is given by [14]

$$u(j\omega) = H(j\omega)[1+G(j\omega)H(j\omega)]^{-1}d(j\omega). \tag{20}$$

For the DVFB control strategy, the controller is assumed to be a constant gain, so that $H(j\omega)=h$, where h is the feedback gain. If the actuator and sensor pair is *point-collocated*, then the plant frequency response $G(j\omega)$ is strictly positive real (SPR), since the total power supplied to the uncontrolled system by the actuator must be positive [13,28]. If a uniform force actuator and a volume velocity sensor are used for the control, then $u(j\omega)=f(j\omega)$, where $f(j\omega)$ is the applied force and $y(j\omega)=Q(j\omega)$, where $Q(j\omega)$ is the measured volume velocity, and the power supplied by the actuator to the system at a frequency ω can be expressed as

$$\Pi(\omega) = \frac{1}{2}\mathrm{Re}[f^{*}(j\omega)Q(j\omega)], \tag{21}$$

where f^* is the complex conjugate of the applied force. Since $Q(j\omega) = G(j\omega)f(j\omega)$, equation (21) can be written as

$$\Pi(\omega) = \frac{1}{2}|f(j\omega)|^2 \,\mathrm{Re}[G(j\omega)] \tag{22}$$

Since the system is *passive*, and therefore the power input is positive at all frequencies and so, according to equation (22), the real part of the plant FRF $G(j\omega)$, in this case *mobility*, must be positive as well [13]. The controller is designed to have a positive definite real part at all frequencies since $H(j\omega) = h$ and $h > 0$.

Thus the plant of the sensor-actuator and the controller FRF are both SPR so that the velocity feedback control system in Figure 4 is *unconditionally stable* [29]. Therefore the feedback gain can be increased, in principle, to infinity in order to drive to zero the signal from the control sensor. In practice, the system under study only approximates a volume velocity sensor and uniform force actuator so that its open-loop FRF $G(j\omega)H(j\omega)$ has to be analysed with reference to the Nyquist stability condition.

5. ANALYTICAL MODELLING OF THE PLANT

When the panel is clamped (C-C-C-C) and subject to transverse vibration, the harmonic out-of-plane velocity at the *k-th* accelerometer point of *K* points on the panel [See Table 1.] can be given as

$$v_k(x_k, y_k, \omega) = j\omega \sum_{m,n} B_{mn}(\omega)\phi_{mn}(x_k, y_k), \tag{23}$$

where for a uniform out-of-plane force excitation $f_u(\omega)$, the modal amplitude $B_{mn}(\omega)$ is given by

$$B_{mn}(\omega) = \frac{\int_0^{L_y}\int_0^{L_x} f_u(\omega)\phi_{mn}(x,y)dxdy}{\Lambda_{mn}[\omega_{mn}^2(1+j\eta_s) - \omega^2]}, \tag{24}$$

where η_s is the hysteresis loss factor of the panel and the normalisation factor Λ_{mn} can be written as [30]

$$\Lambda_{mn} = \rho_s(2h_s)^2 \int_0^{L_y}\int_0^{L_x} \phi_{mn}^2(x,y)dxdy = \rho_s h_s^2 L_x L_y. \tag{25}$$

The m,n*-th* out-of-plane natural frequency ω_{mn} of the panel is expressed as [31]

$$\omega_{mn} = \frac{\pi^2 h_s}{L_y^2}\left\{\frac{Y_s\alpha}{3\rho_s(1-\nu_s^2)}\right\}^{1/2}, \tag{26}$$

where α is given by [31]

$$\alpha = G_x^4 + G_y^4\left(\frac{a}{b}\right)^4 + 2\left(\frac{a}{b}\right)^2[\nu_s H_x H_y + (1-\nu_s)J_x J_y], \tag{27}$$

and the variables G_x, G_y, H_x, H_y, J_x, and J_y are defined for the *x*-directional mode number *m* for a clamped (C-C-C-C) panel as [32]

$$\begin{aligned} m = 1 \qquad & G_x = 1.506, \;\; H_x = J_x = 1.248 \\ m \geq 2 \qquad & G_x = m + 0.5, \;\; H_x = J_x = (m+0.5)^2\left[1 - \frac{2}{(m+0.5)\pi}\right], \end{aligned} \tag{28}$$

while for the *y*-directional mode number *n*

(29)

$$n=1 \qquad G_y=1.506,\ \ H_y=J_y=1.248$$

$$n\geq 2 \qquad G_y=n+0.5,\ \ H_y=J_y=(n+0.5)^2\left[1-\frac{2}{(n+0.5)\pi}\right].$$

The harmonic out-of-plane velocity can be rewritten from equations (23) and (24) as

$$v_k(x_k,y_k,\omega)=j\omega\sum_{m,n}f_u(\omega)C_{mn}D_{mn}\phi_{mn}(x_k,y_k), \tag{30}$$

where $C_{mn}=\int_0^{L_y}\int_0^{L_x}\phi_{mn}(x,y)dxdy$ and $D_{mn}=\frac{1}{\Lambda_{mn}[\omega_{mn}^2(1+j\eta_s)-\omega^2]}$. The out-of-plane mode of the panel can be calculated by the product of the two beam functions, $\phi_{mn}(x_k,y_k)=\phi_m(x_k)\phi_n(y_k)$, as described in the reference [31]. After some manipulation, the coefficient C_{mn} has been found to be [13]:

$$C_{mn}=\frac{16L_xL_y}{\gamma_m\gamma_n}\sin\left(\frac{\gamma_m}{2}\right)\sin\left(\frac{\gamma_n}{2}\right), \tag{31}$$

where $m,n=1,3,5,\ldots$ and the constant γ_i can be calculated from the following equations [31]

$$\begin{aligned}&\tan\frac{1}{2}\gamma_i+\tanh\frac{1}{2}\gamma_i=0 \qquad \text{for odd modes} \quad i=1,3,5,\ldots\\ &\tan\frac{1}{2}\gamma_i'-\tanh\frac{1}{2}\gamma_i'=0 \qquad \text{for even modes} \quad i=2,4,6,\ldots\end{aligned} \tag{32}$$

The reconstructed volume velocity of a panel using regularly distributed *K* point velocity sensors can be given as

$$\tilde{Q}(\omega)=\sum_{k=1}^{K}v_k(x_k,y_k,\omega) \tag{33}$$

Thus the plant $G(t)$ of this smart panel system can be analytically expressed, using equation (12), with

$$G(\omega)=\frac{\tilde{Q}(\omega)}{V_3(\omega)}=-h_{act}L_{pe}[S(x,y)]\sum_{k=1}^{K}\left[j\omega\sum_{m,n}C_{mn}D_{mn}\phi_{mn}(x_k,y_k)\right] \tag{34}$$

6. MEASURED AND CALCULATED PLANT FREQUENCY RESPONSE FUNCTIONS

The measured plant FRF, i.e. output sum of velocities per unit input voltage to the uniform force actuator, is shown in Figure 5. A gradual decreasing magnitude trend with the increase of frequency up to 10000Hz can be found. Comparing the plant FRF of the matched PVDF sensor-actuator pair in Figure 2 with that in Figure 5, it is found that the plant FRF with the configuration of the PVDF actuator and the 4×4 accelerometers array is not coupled via in-plane vibration of the panel.

The sensor-actuator FRF at a lower frequency range is plotted in Figure 6. Since some shaping errors have been highlighted for the quadratically shaped electrodes of the PVDF actuator, the measured (*thick line*) and calculated (designed actuator shape: *dashed line*, erroneous actuator shape: *thin line*) plant FRFs between 0 and 2000Hz are compared as shown in Figure 6.

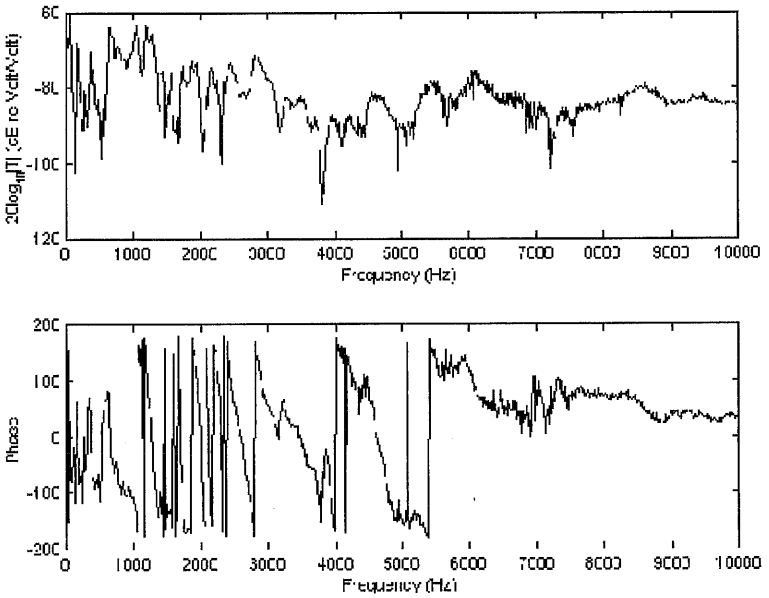

Figure 5. Measured FRF (0 - 10000Hz) of a smart panel with a PVDF actuator and a 4×4 accelerometers array.

The calculated plant FRF with the designed PVDF actuator shape shows a continuous reduction of the magnitude with frequency. The phase response lies between $\pm 90^{\circ}$ up to about 900Hz. Above 900Hz the phase response is characterised by a phase lag with an anti-resonance at the frequency of about 1100Hz. This is caused by aliasing problems due to the limited number of accelerometers used to reconstruct the volume velocity of the panel. The measured FRF shows the typical feature of driving point mobility below about 350Hz [33], which includes the first three odd bending modes of the panel that largely contribute to the low frequency sound radiation.

The resonances are alternated by anti-resonances that occur at frequencies quite close to the following resonance. Also the phase response lies between $\pm 90^{\circ}$ and the magnitude tends to decrease with frequency. However, the measured FRF between about 350Hz and 900Hz shows two unexpected higher peaks in correspondence to the resonance frequencies of the fourth and fifth modes. Beyond about 900Hz, the measured sensor-actuator FRF is characterised by sharp resonances with phase lags. The two sharp resonances located at about 1000Hz - 1200Hz are high enough to cause instability of the feedback control system when a high feedback gain is used. The calculated FRF with the erroneous shaped actuator shows a similar trend to the measured one. This indicates that the measured two peaky resonances at about 1000Hz - 1200Hz may be caused by the shaping error of the PVDF actuator.

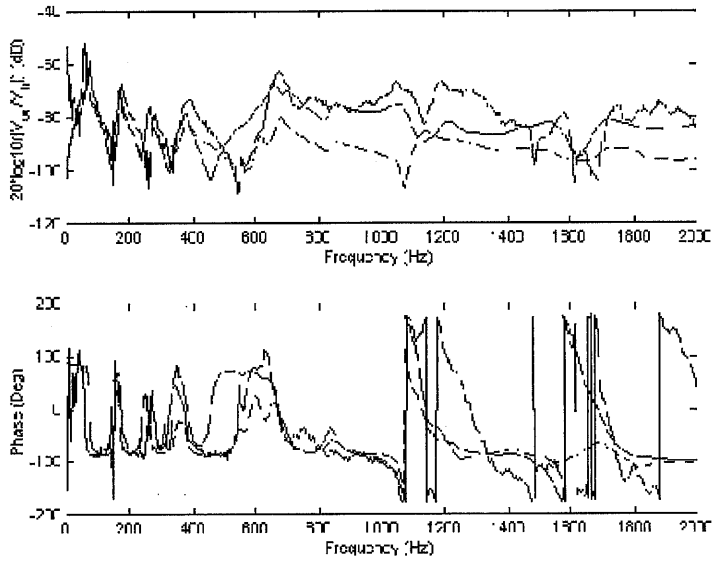

Figure 6. FRFs at 0 - 2000Hz of a smart panel with a PVDF actuator and a 4×4 accelerometer array. *Thick line*: measured FRF. *Dashed line*: calculated FRF with the designed actuator shape. *Thin line*: calculated FRF for the actuator shape with errors.

The observed shape function with errors $\hat{S}(x,y)$ has been defined with a 9-th order polynomial, as shown in Figure 7(a), where the designed shape is given by the quadratic function in equation (10). Since $\hat{S}(x,y)$ does not give the results found in equation (11), the out-of-plane force of the shape with errors has been written by

$$\hat{f}_u(t) = -h_{act} e_{31} V_3(t) \frac{\partial^2 \hat{S}(x,y)}{\partial x^2} \quad (35)$$

The out-of-plane force distributions of the designed shaped actuator $f_u(t)$ (thin line) and the actuator with errors $\hat{f}_u(t)$ (thick line) are compared in Figure 7(b), which shows that $\hat{f}_u(t)$ does not generate uniform out-of-plane force.

The normalised force distribution shows that the actuator with errors produces an excitation at the tip position about 27 times bigger than that produced by the designed actuator. Also the shaped actuator with errors generates negative forces. This non-uniform force distribution causes the two sharp resonances at about 1000 - 1200Hz with extra phase lags as plotted in Figure 6. Thus the configuration of the smart panel with the PVDF actuator having shaping errors, and an array of 4×4 accelerometers gives SPR property below about 900Hz so that a *conditionally stable* SISO controller only can be implemented. The feedback gain in the control system must be limited because of the two sharp peaks at about 1000 - 1200Hz. The shaping error of the piezoelectric actuator and the aliasing problem related to the discretised detection of the volume velocity can limit the stability of a feedback control.

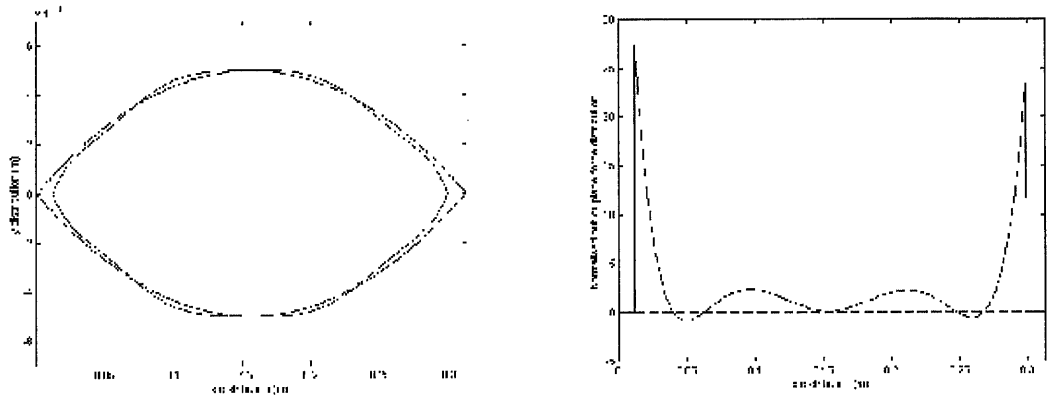

(a) (b)

Figure 7. Comparison of the designed (thin line) and actual (thick line) PVDF actuator strips. (a) Shapes of a PVDF actuator strip. (b) Comparison of the out-of-plane force distributions after normalisation.

7. ACOUSTICAL CONTROL USING VELOCITY FEEDBACK

Since the smart panel can not provide SPR property at all frequencies, a limited positive feedback gain is chosen to implement a conditionally stable feedback controller. The stability of the control system has been determined by examining the locus of the measured open-loop FRF $G(j\omega)H(j\omega)$ up to 100kHz. In the experiment, a PCB power amplifier provides the feedback control gain input to the PVDF actuator.

Figure 8 shows the measured volume velocity with (*dashed line*) and without (*solid line*) control when the panel is excited with the acoustic field (white noise) generated by the loudspeaker in the wooden box. The volume velocity is estimated with the array of accelerometers in which case the gain margin is found to be of about 6dB. The volume velocity attenuation of about 15dB at the resonance frequency of the first mode has been achieved. The volume velocity attenuation for resonance of the second mode is about 6dB and that of the third mode is about 5dB. The attenuation between the resonance of the third mode and 1000Hz is of the order of about 5dB as well.

The sound transmission control experiment has been carried out with the same feedback gain. In this experiment, a B&K Type 4165 1/2" microphone has been used to measure the radiated sound pressure from the panel. The B&K microphone has been installed about 10cm above the panel in correspondence to its centre. The signal from the microphone is connected to an Advantest FFT analyser via a B&K Type 2609 microphone amplifier.

Figure 9 shows the measured sound pressure with (*dashed line*) and without (*solid line*) control. The attenuation of the sound transmission for the resonance frequency of the first mode is about 8dB and about 5 dB for both the second and third modes. The controlled FRF between the third mode and about 800Hz maintains small attenuation as well, however the enhancement has been found at higher frequencies, especially at the resonances in about 800 - 900Hz.

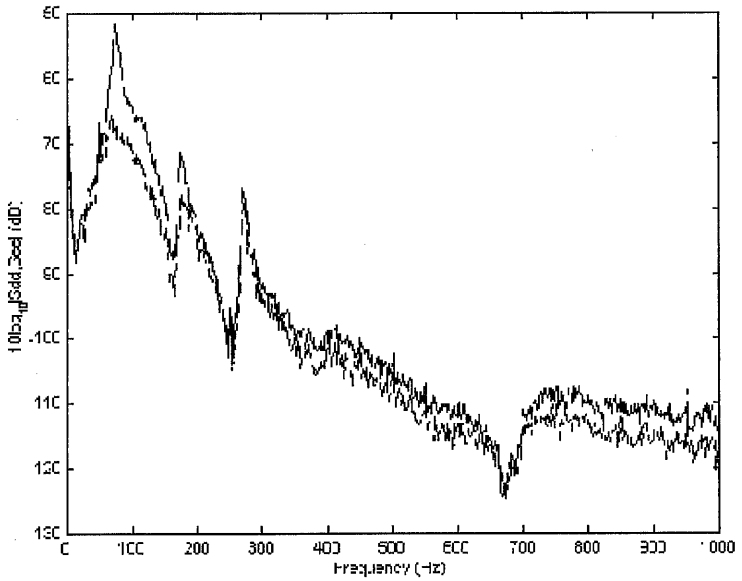

Figure 8. The measured vibration control result of the smart panel when the accelerometers array is used as an error sensor with the limited gain feedback controller. Before control: *dashed line* and after control: *solid line*.

Since the sound transmission control has been carried out with the smart panel clamped on a wooden box in a general experimental lab, more exact measurement could be achieved when the testing rig is used in an anechoic chamber. The attenuation measured with this experiment could be improved by the use of a phase lag compensator [34], which could modify the open-loop FRF of the plant at the frequency range about 1000 - 1200Hz.

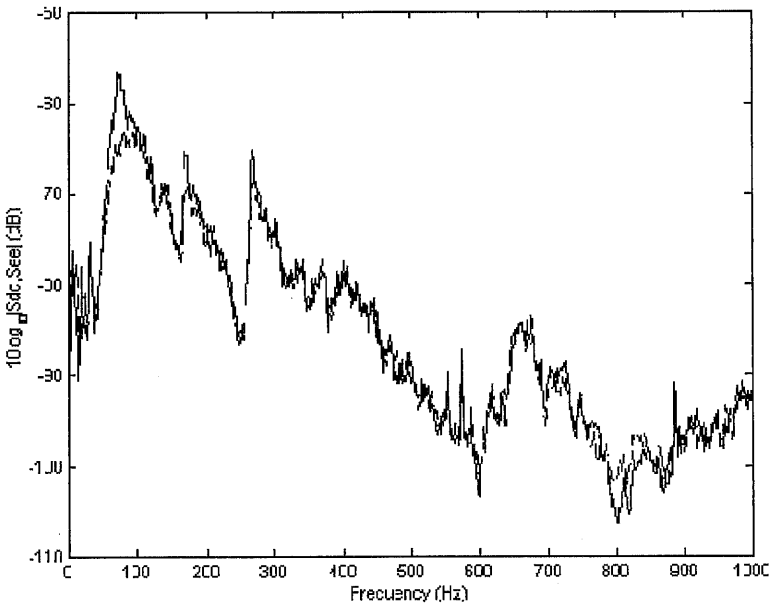

Figure 9. The measured acoustic transmission control result of the smart panel when the accelerometers array is used as an error sensor with the limited gain feedback controller. Before control: *dashed line* and after control: *solid line*.

8. CONCLUSIONS

This paper reports a study of low frequencies volume velocity control of a smart panel for the reduction of sound transmission through a smart panel. The smart panel is a clamped aluminium rectangular plate with the dimension of 414×313×1 mm. The panel has an array of quadratically shaped PVDF actuators that exert a uniform transverse force and an array of 4×4 accelerometers that reconstructs the volumetric vibration of the panel. This smart panel is designed to provide a single-input and single-output (SISO) system so that direct velocity feedback control can be applied. At low frequencies the measured FRF of the plant shows a gradual decreasing magnitude with the increase of frequency. This confirms that this sensor-actuator pair is not affected by the in-plane coupling found with a matched piezoelectric sensor-actuator pair. However, two unexpected sharp peaks and phase lags at about 1000 - 1200Hz have been observed. It has been found that this is partially caused by the shaping error of the PVDF actuator and partially caused by aliasing problems of the discretised sensor. These two sharp peaks could cause the instability of the feedback control system. With a simple direct velocity feedback control system, the attenuations of about 15dB in vibration level and about 8dB in acoustic power level at the resonance frequency of the first mode of the smart panel have been achieved.

Acknowledgements

The smart panel used in this work was constructed under the EU DAFNOR (*Distributed Active Foils for NOise Reduction*) project. The authors would like to thank Thomson Marconi who built the smart panel.

References

1. F. Fahy, 1985, *Sound and Structural Vibration: Radiation, Transmission and Response*, Academic Press.
2. D. J. Mead, 1999, *Passive Vibration Control*, John Wiley & Sons.
3. P. A. Nelson and S. J. Elliott, 1992, *Active Control of Sound*, Academic Press.
4. C. R. Fuller, S. J. Elliott, and P. A. Nelson, 1996, *Active Control of Vibration*, Academic Press.
5. A. Preumont, 1997, *Vibration Control of Active Structures: An Introduction,* Kluwer Academic Publishers.
6. R. L. Clark, W. R. Saunders, and G. P. Gibbs, 1998, *Adaptive Structures Dynamics and Control*, John Wiley & Sons.
7. C. R. Fuller and R. J. Silcox, 1995, *Journal of Acoustical Society of America*, **91**(1), 519, Active structural acoustic control.
8. M. E. Johnson and S. J. Elliott, 1995, *Journal of Acoustical Society of America*, **98**(4), 2174-2186, Active control of sound radiation using volume velocity cancellation.
9. J. Rex and S. J. Elliott, 1992, *Proceedings of MOVIC*, 339-343, The QWSIS-A new sensor for structural radiation control.
10. F. Charette, A. Berry, and C. Guigou, 1998, *Journal of the Acoustical Society of America*, **103**(3), 1493-1503, Active control of sound radiation from a plate using a polyvinylidene fluoride volume displacement sensor.
11. A. Preumont, A. Francois, and S. Debru, 1999, *ASME Journal of Vibration and Acoustics*, **121**, 446-452, Piezoelectric array sensing for real-time, broad-band sound radiation measurement.
12. M. J. Balas, 1979, *Journal of Guidance and Control*, **2**(3), 252-253, Direct velocity feedback control of large space structures.
13. P Gardonio, Y-S Lee, S J Elliott, and S Debost, 2001, *Journal of Aerospace Engineering, Proceedings of the Institution of Mechanical Engineers Part G*, **215**, 187-206, A panel with matched PVDF volume velocity sensor and uniform force actuator for the active control of sound transmission.
14. S. J. Elliott, 2001, *Signal Processing for Active Control*, Academic Press.
15. Y.-S. Lee, 2000, *Active control of smart structures using distributed piezoelectric transducers*, PhD thesis, University of Southampton.
16. D. G. Cole, W. R. Saunders and H. H. Robertshaw, 1995, *ASME Journal of Vibration and Acoustics*, **117**, 431-438, Modal parameter estimation for piezostructures.
17. S. Y. Yang and W. H. Huang, 1998, *Journal of Sound and Vibration*, **216**(3), 529-538, Is a collocated piezoelectric sensor/actuator pair feasible for an intelligent beam.
18. E. H. Anderson and N. W. Hagood, 1992, *AIAA-92-2465-CP*, Self-sensing piezoelectric actuation: Analysis and application to controlled structures.
19. J. S. Vipperman and R. L. Clark, 1996, *AIAA Journal*, **34**(10), 2102-2109, Implementation of adaptive piezoelectric sensoriactuator.
20. Y.-S. Lee, S. J. Elliott and P. Gardonio, 2001, *8th SPIE Smart Structures and Materials, Newport Beach, California, USA*, Distributed four-layer PVDF actuator/sensor arrangement for the control of beam motion.

21. J. P. Maillard and C. R. Fuller, 1998, *Journal of Acoustical Society of America*, **103**(1), 396 - 400, Comparison of two structural sensing approaches for active structural acoustic control.
22. C. K. Lee, 1990, *Journal of Acoustical Society of America*, **87**(3), 1144-1158, Theory of laminated piezoelectric plates for the design of distributed sensors/actuators. Part I: Governing equations and reciprocal relationships.
23. IEEE, 1988, *Standard on Piezoelectricity*, ANSI/IEEE Std 176-1987.
24. G. B. Warburton, 1976, *The Dynamical Behaviour of Structures (2nd Ed.),* Pergamon Press.
25. T. J. Sutton, M. E. Johnson and S. J. Elliott, 1997, *Proceedings of 6th International Conference on Recent Advances in Structural Dynamics*, 1247-1255, A distributed actuator for the active control of sound transmission through a partition.
26. S. J. Elliott and M. E. Johnson, 1993, *Journal of Acoustical Society of America*, **94**(4), 2194-2204, Radiation modes and the active control of sound power.
27. S. P. Bhattacharyya, H. Chapellat, and L. H. Keel, 1995, *Robust Control: The Parametric Approach*, Prentice-Hall.
28. S. J. Elliott, P. Gardonio, T. J. Sors, and M. J. Brennan, 2001, *8th SPIE Smart Structures and Materials, Newport Beach, California, USA*, Active vibro-acoustic control with multiple local feedback loops.
29. S. M. Joshi, 1989, *Control of Large Flexible Space Structures,* Springer-Verlag.
30. P. Gardonio and S. J. Elliott, 1998, *Driving point and transfer mobility matrices for thin plates excited in flexure*, ISVR Technical Report No.277, University of Southampton.
31. G. B. Warburton, 1951, *Proceedings of the Institute of Mechanical Engineering*, **168**, 371-384, The vibration of rectangular plates.
32. A. W. Leissa, 1969, *Vibration of Plates*, NASA.
33. D. J. Ewins, 1984, *Modal Testing: Theory and Practice*, John Wiley & Sons.
34. G. F. Franklin, J. D. Powell, and A. Emami-Naeini, 1994, *Feedback Control of Dynamic Systems (3rd ed.)*, Addison-Wesley.